

Astrophysical properties of star clusters projected toward tidally perturbed SMC regions

Denis M.F. Illesca^{1,2*}, Andrés E. Piatti^{1,2}, Matías Chiarpotti^{1,2}, and Roberto Butrón¹

¹ Instituto Interdisciplinario de Ciencias Básicas (ICB), CONICET-UNCUYO, Padre J. Contreras 1300, M5502JMA, Mendoza, Argentina;

² Consejo Nacional de Investigaciones Científicas y Técnicas (CONICET), Godoy Cruz 2290, C1425FQB, Buenos Aires, Argentina

Received / Accepted

ABSTRACT

We report on the astrophysical properties of a sample of star clusters in the Small Magellanic Cloud (SMC). They have been selected with the aim of looking for the connection between their ages, heliocentric distances and metallicities with the existence of tidally perturbed/induced outermost SMC regions. We derived the star cluster fundamental parameters from relatively deep Survey of the Magellanic Stellar History (SMASH) DR2 color-magnitude diagrams (CMDs), cleaned from field star contamination, and compared to thousand synthetic CMDs covering a wide range of heliocentric distances, ages and metal content. Heliocentric distances for 15 star clusters are derived for the first time, which represents an increase of ~50 per cent of SMC clusters with estimated heliocentric distances. The analysis of the age-metallicity relationships (AMRs) of cluster located in outermost regions distributed around the SMC and in the SMC Main Body reveals that they have followed the overall galaxy chemical enrichment history. However, since half of the studied clusters are placed in front of or behind the SMC Main Body, we concluded that they formed in the SMC and have traveled outward because of the tidal effects from the interaction with the Large Magellanic Cloud (LMC). Furthermore, metal-rich clusters formed recently in some of these outermost regions from gas that was also dragged by tidal effects from the inner SMC. This outcome leads to consider the SMC as a galaxy scarred by the LMC tidal interaction with distance-perturbed and newly induced outermost stellar substructures.

Key words. Methods: data analysis – Techniques: photometric – Galaxies: individual: Small Magellanic Cloud – Galaxies: star clusters: general

1. Introduction

The Magellanic Clouds is a pair of interacting irregular dwarf galaxies that are experiencing their first passages close to the Milky Way (Kallivayalil et al. 2013). Indeed, since recent years, some trails of the tidal effects on them have been observed. In the case of the Small Magellanic Cloud (SMC) several efforts have been made with the aim of precisely tracing its internal kinematic behavior (Niederhofer et al. 2018; Zivick et al. 2018; Di Teodoro et al. 2019, , and references therein). However, depending on the stellar population chosen and the observational data used, such tidal perturbations turned out to be of different magnitude (De Leo et al. 2020; Zivick et al. 2021; Niederhofer et al. 2021). As far as we are aware, tidal effects have been found to be stronger in the outermost galaxy regions, particularly those facing to the other interacting galaxy, while they are close to each other (Almeida et al. 2024; Cullinane et al. 2023). Until now, SMC star clusters have not been extensively used as tracers of the internal kinematics of this galaxy (Maia et al. 2019; Piatti 2021). However, they present several advantages from different points of view. For instance, their mean radial velocities and proper motions come from the average of several measurements of cluster members, thus resulting in mean values based on a sound statistics. Star clusters are also appropriate representatives of the internal motion in the SMC, compared to the radial velocities and mean proper motions of stars aligned along differ-

ent lines of sight through it. This is also valid even when it comes from the separate analysis of different stellar populations of the galaxy field. On the other hand, star clusters have precisely determined ages and distances, so that the internal kinematics of the SMC can be easily linked to the metallicities of the star clusters, and thus provide an adequate framework for our understanding of their formation and chemical and kinematic evolution of the galaxy.

By studying SMC star clusters distributed across the Southern Bridge, the SMC Wing, the West Halo, the Counter Bridge (Dias et al. 2014), among other tidally perturbed/induced SMC stellar substructures, it is possible to shed light on the origin of such stellar substructures, on their dimensions and their location with respect to the SMC Main Body, their chemistry and their epoch of formation (see, e.g. Piatti 2022). Precisely, we have embarked in an effort of homogeneously estimating astrophysical properties (e.g., heliocentric distances, ages, and metallicities) of star clusters distributed in those SMC selected regions, aiming at performing an overall analysis of the magnitude of the tidal effects throughout the whole galaxy. We particularly focus on the estimation, for the first time, of star cluster heliocentric distances, which are remarkably lacking in the literature (Piatti 2023). During several decades, SMC star clusters were thought to be located at the mean galaxy distance, with the consequent misleading in the interpretation of their formation history in the galaxy. However, several studies have shown that the SMC is much more extended along the line of sight than its ap-

* e-mail: denisillesca1113@gmail.com

Table 1. Averaged literature values of fundamental parameters of the studied star clusters.

Star Cluster	$(m - M)_0$ (mag)	Log(age /yr)	[Fe/H] (dex)	Method	References
B88	19.0 ± 0.10	8.12 ± 0.22	-0.25 ± 0.15	Photometry	1;2
B99	—	8.10 ± 0.01	-0.84 ± 0.04	Photometry; CaII triplet	5;6
B139	19.10 ± 0.11	8.06 ± 0.12	-0.30 ± 0.24	Photometry	1;2
B168	18.96 ± 0.07	9.82 ± 0.06	-1.08 ± 0.06	Photometry; CaII triplet	3;4
BS116	18.75 ± 0.12	9.27 ± 0.07	-0.77 ± 0.12	Photometry	1
BS121	—	9.45 ± 0.08	-0.66 ± 0.07	CaII triplet	7;8
BS188	18.61 ± 0.12	9.26 ± 0.05	-0.94 ± 0.06	Photometry; CaII triplet	3;4
H86-97	—	8.50 ± 0.02	-0.70 ± 0.04	Photometry; CaII triplet	6;9
HW31	—	9.28 ± 0.11	-0.89 ± 0.04	CaII triplet; Photometry	2;8;10
HW41	—	9.38 ± 0.29	-0.67 ± 0.05	CaII triplet; Photometry	2;8;10
HW47	—	9.48 ± 0.07	-0.96 ± 0.22	CaII triplet; Photometry	8;11;12
HW56	18.69 ± 0.09	9.47 ± 0.04	-0.90 ± 0.14	Photometry; CaII triplet	1;4
HW64	19.19 ± 0.08	7.47 ± 0.31	-0.38 ± 0.20	Photometry	1
HW67	18.71 ± 0.13	9.35 ± 0.05	-0.74 ± 0.12	Photometry; CaII triplet	1;6
HW73	19.18 ± 0.04	8.01 ± 0.08	-0.32 ± 0.22	Photometry	1;2
HW77	18.83 ± 0.12	9.05 ± 0.04	-1.02 ± 0.11	Photometry	13
HW84	—	9.29 ± 0.05	-0.90 ± 0.05	Photometry	7;8;12
HW86	18.53 ± 0.09	9.15 ± 0.05	-0.65 ± 0.09	CaII triplet; Photometry	7;8;14
IC1655	18.66 ± 0.04	8.18 ± 0.20	-0.61 ± 0.18	Photometry	1;2
L2	18.72 ± 0.10	9.59 ± 0.02	-1.29 ± 0.13	Photometry; CaT lines	13;21;22
L3	18.64 ± 0.14	9.08 ± 0.11	-0.75 ± 0.33	Photometry	10;21;24
L4	18.65 ± 0.10	9.90 ± 0.06	-1.08 ± 0.04	Photometry; CaII triplet	3;7;8
L6	18.70 ± 0.09	9.94 ± 0.06	-1.24 ± 0.03	Photometry; CaII triplet	3;7;8
L7	—	9.17 ± 0.04	-0.82 ± 0.06	CaII triplet; Photometry	6;7;20
L9	18.93 ± 0.07	9.22 ± 0.07	-0.66 ± 0.01	Photometry; CaII triplet	6;12;13
L11	—	9.48 ± 0.06	-1.07 ± 0.18	Deep Photometry; CaII triplet	7;8;15
L13	18.66 ± 0.04	8.75 ± 0.08	-1.05 ± 0.06	Photometry; CaII triplet	6;13;18
L17	—	9.64 ± 0.06	-0.84 ± 0.03	CaII triplet	7;8
L19	—	9.48 ± 0.03	-0.87 ± 0.02	Photometry; CaII triplet	1;19;20
L27	18.84 ± 0.10	9.55 ± 0.06	-1.01 ± 0.10	Photometry; CaII triplet	2;3;7;19;22;23
L58	—	9.13 ± 0.28	-0.78 ± 0.02	Photometry; CaII triplet	2;6;25
L73	18.83 ± 0.13	9.27 ± 0.04	-0.65 ± 0.13	Photometry	1
L95	19.18 ± 0.10	7.94 ± 0.34	-0.36 ± 0.27	Photometry	1;2
L100	18.81 ± 0.06	9.46 ± 0.04	-0.75 ± 0.08	Photometry; CaII triplet	1;4;11
L108	—	9.27 ± 0.09	-0.88 ± 0.18	CaII triplet; Photometry	7;8
L110	18.95 ± 0.10	9.88 ± 0.06	-1.03 ± 0.05	Photometry; CaII triplet	14;7;8
L116	—	9.44 ± 0.20	-1.0 ± 0.11	Photometry; CaII triplet	16;17
NGC416	18.96 ± 0.07	9.78 ± 0.04	-0.85 ± 0.04	Photometry; CaII triplet	23;21;26
NGC458	18.74 ± 0.03	8.14 ± 0.07	-0.39 ± 0.08	Photometry	1;27
OGLE-SMC 133	—	9.80 ± 0.40	-0.80 ± 0.07	Photometry; CaII triplet	2;6

References. (1) Piatti (2022); (2) Glatt et al. (2010); (3) Piatti (2022); (4) Dias et al. (2021); (5) Maia et al. (2014); (6) Parisi et al. (2015); (7) Parisi et al. (2009); (8) Parisi et al. (2014); (9) Chiosi et al. (2006); (10) De Bortoli et al. (2022); (11) Parisi et al. (2022); (12) Piatti et al. (2005); (13) Saroon et al. (2023); (14) Oliveira et al. (2023); (15) Livanou et al. (2013); (16) Piatti et al. (2001); (17) Parisi et al. (2022); (18) Nayak et al. (2018); (19) Narloch et al. (2021); (20) Gatto et al. (2021); (21) De Grijs & Bono (2015); (22) Dias et al. (2022); (23) Milone et al. (2023); (24) Dias et al. (2014); (25) Maia et al. (2019); (26) Glatt et al. (2008); (27) Alcaïno et al. (2003).

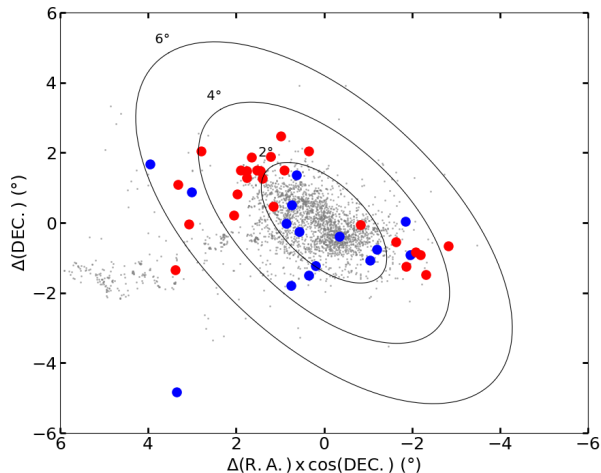


Fig. 1. Spatial distribution of SMC clusters (Bica et al. 2020) represented with gray points. Red and blue filled circles represent the studied clusters with or without previous estimates of their heliocentric distances, respectively. The ellipses correspond to the framework devised by Piatti et al. (2007) for $a = 2^\circ, 4^\circ,$ and $6^\circ,$ respectively.

parent size projected in the sky (Ripepi et al. 2017; Graczyk et al. 2020), which makes meaningful to derive accurate heliocentric distances.

This work is organized as follows: Section 2 describes the selection of the star cluster sample, alongside with the data used in the analysis, the assignment of cluster star membership, and the estimation of the cluster astrophysics parameters, namely, reddening, age, distance and metallicity. Section 3 deals with the resulting clusters' properties, while in Section 4 we analyze them to the light of the SMC stellar spatial distribution and star formation history. Section 5 summarizes the main conclusions of this work.

2. Observational data

We selected 40 star clusters mainly distributed across the outer SMC regions using the catalog compiled by Bica et al. (2020). Table 1 gathers the most relevant fundamental parameters available in the literature, alongside with the method employed to derive them. We used as reference the framework devised by Piatti et al. (2007), which consists of concentric equally aligned ellipses, with a position angle of 54° (measured anti-clockwise from the North) and a ratio between the semi-major to the semi-minor axes of 2. The selected star clusters are preferentially located outside the area covered by an ellipse with a semi-major axis of 2° . As mentioned in Section 1, they populate known perturbed/induced stellar substructures. Figure 1 illustrates the spatial distribution of the selected cluster sample, where fifteen clusters that have not been targeted for estimating their heliocentric distances until now are highlighted with blue symbols.

Considering the overall low brightness and compactness of the selected star clusters, the relatively deep photometric data provided by the Data Release 2 of the Survey of the Magellanic Stellar History (SMASH, Nidever et al. 2021) is suitable to perform an homogeneous estimation of their astrophysical parameters. Its limiting magnitude is beyond the 24th magnitude in the outskirts of the SMC, which is several magnitudes underneath the Main Sequence turnoff of a ~ 1 Gyr old cluster located at

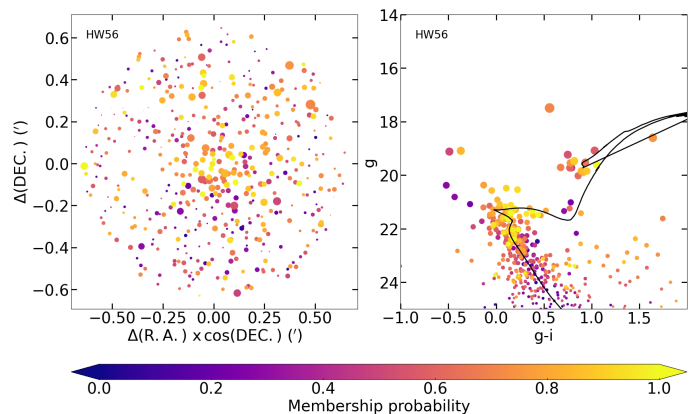


Fig. 2. **Left:** schematic finding chart of HW 56. The size of the symbols are proportional to the star brightness. **Right:** Cluster color-magnitude diagram with the theoretical isochrone (Bressan et al. 2012) corresponding to the adopted cluster parameters superimposed (see Table 2). The color bar indicates the membership probability.

the distance of the SMC. The data of each selected cluster were retrieved from the Astro Data Lab¹ interface, which is part of the Community Science and Data Center at NSF's National Optical Infrared Astronomy Research Laboratory. Particularly, we were interested in the R.A and Dec. coordinates, the PSF g, i magnitudes and their respective errors, the $E(B - V)$ interstellar reddening and χ and SHARPNESS parameters of stellar sources located inside a circular region with a radius six times that of the cluster (Bica et al. 2020). With the aim of minimizing the contamination of bad pixels, cosmic rays, background galaxies, and unrecognized double stars, we selected those sources with $0.2 \leq \text{SHARPNESS} \leq 1.0$ and $\chi < 0.5$.

Aiming at disentangling the main features of the observed cluster color-magnitude diagrams (CMDs), we first cleaned them from star field contamination on a statistical basis using the procedure devised by Piatti & Bica (2012). It uses the magnitude and color of each star in the so-called reference star field CMD and finds the closest one in magnitude and color in the cluster's CMD and subtracts it. We used the reddening corrected g_0, i_0 magnitudes computed from the observed g, i magnitudes, the $E(B - V)$ values retrieved from SMASH and the $A_\lambda/E(B - V)$ ratios, for $\lambda = g, i$, given by Abott et al. (2018). In practice, (1) we selected stars located within the cluster circle with a radius equal the cluster's radius (Bica et al. 2020), and built the respective CMD; (2) we constructed a thousand CMDs with an area equal to the cluster circle and randomly located at a distance from the cluster center equals to 4.5 times the cluster's radius; (3) we performed the subtraction from the cluster's CMD of stars distributed similarly as those in the reference field CMDs, employing in the decontamination process one reference field CMD at a time. Therefore, we generated a thousand different cleaned cluster's CMDs. (4) Finally, we assigned membership probabilities based on the number of times a star survived the cleaning procedure, namely: $P = 1 - N/1000$, where N represents the number of times a star was subtracted. Figure 2 illustrates the resulting membership probability distribution of stars in the field of HW56.

From the field star decontaminated cluster photometry we derived the clusters' properties employing routines of the Automated Stellar Cluster Analysis code (ASteCA, Perren et al. 2015). ASteCA allows to derive simultaneously the metallicity,

¹ <https://datalab.noirlab.edu/splash/splash.php>

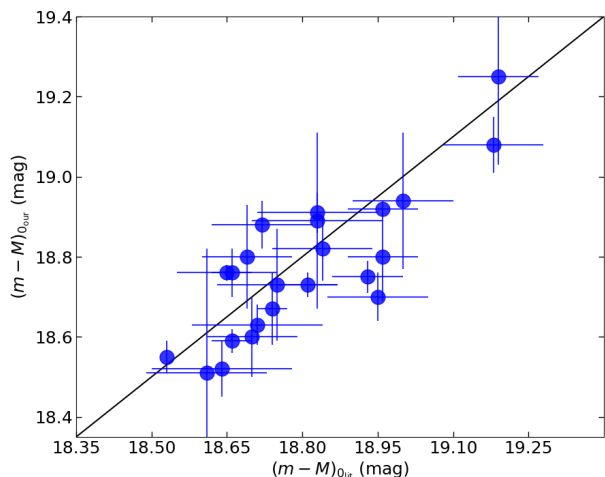


Fig. 3. Comparison between the derived distances moduli and those adopted from the literature. The solid line represents the identity relationship.

the age, the distance, and the cluster present mass by producing a large number of synthetic CMDs and then choosing that that best reproduces the cleaned star cluster CMD. The metallicity, age, distance, cluster present mass and binary fraction associated to that generated synthetic CMD are adopted as the best-fitted cluster properties. In order to generate a statistical significant sample of synthetic CMDs, we adopted the initial mass function of Kroupa (2002) and a minimum mass ratio for the generation of binaries of 0.5. Cluster masses and binary fractions were set in the ranges 100-5000 M_{\odot} and 0.0-0.5, respectively. We also used PARSEC² v1.2S isochrones (Bressan et al. 2012) for the SMASH photometric system, spanning metallicities Z from 0.0001 ($[Fe/H] = -2.18$ dex) up to 0.030 ($[Fe/H] = 0.30$ dex), in steps of $\Delta Z = 0.001$, and $\log(\text{age}/\text{yr})$ from 6.0 (1 Myr) up to 10.1 (12.5 Gyr) in steps $\Delta(\log(\text{age}/\text{yr})) = 0.025$. These metallicity and age ranges embrace the whole SMC age-metallicity relationship (Piatti & Geisler 2013). In some cases, we used smaller range values as prior to secure astrophysically meaningful results. We entered ASteCA with the cluster SMASH photometry and the previously independently assigned membership probabilities to each observed star and derived the aforementioned cluster astrophysical parameters with their respective uncertainties. These errors were estimated from the standard bootstrap method described in Efron (1982). Table 2 lists the resulting cluster parameters, while Figure 2 depicts the CMD of HW56 with the isochrone corresponding to the clusters' parameters superimposed. Similar figures for the remaining cluster sample are included in the Appendix.

3. Star cluster properties

Table 2 shows that the selected cluster sample comprises SMC clusters that span a wide age range (~ 3 Myr - 7.06 Gyr); nearly any known SMC metallicity value ($[Fe/H] \sim -1.3$ dex - -0.25 dex); and a noticeable range of heliocentric distances ($d \sim 36$ kpc - 75 kpc). Although some few clusters are known to have heliocentric distances that place them outside the Main Body of the SMC (~ 56 -62 kpc, see Piatti 2022), we here found nearly 10

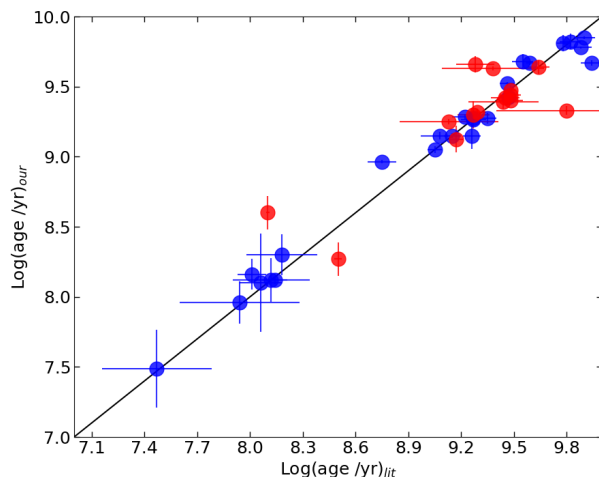


Fig. 4. Comparison between the derived ages and those adopted from the literature. Blue filled circles represent star clusters with previous estimates of their heliocentric distances, while red filled circles correspond to those without such estimates. The solid line represents the identity relation.

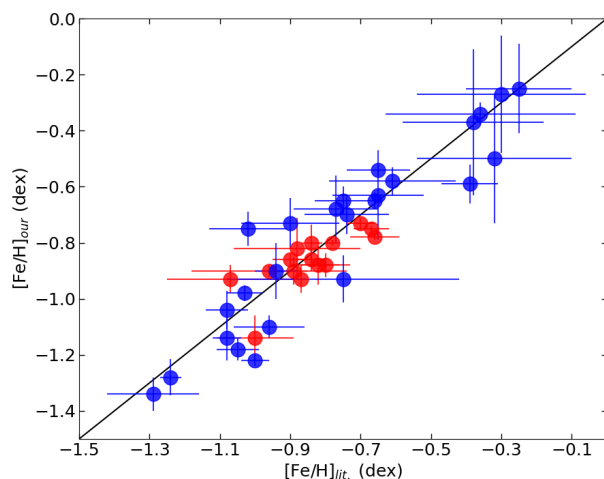


Fig. 5. Comparison between the derived metallicities and those adopted from the literature. Blue filled circles represent star clusters with previous estimates of their heliocentric distances, while red filled circles correspond to those without such estimates. The solid line represents the identity relation.

additional clusters also located in the SMC periphery. Because of the impact of these new heliocentric distances in our knowledge of the formation and evolution of the SMC, we first validated our resulting astrophysical parameters by comparing them with those available in the literature (see Table 1).

Previous estimates of metallicity, age and heliocentric distance of the studied cluster sample were thoroughly sought in the available literature. For clusters with more than one estimate, we averaged the published values, giving more weight to spectroscopic metallicities than those obtained from theoretical isochrone fitting to the clusters' CMDs. Whenever ages or heliocentric distances derived from CMD analyses are available, those from deeper and higher quality photometry were assigned

² <http://stev.oapd.inaf.it/cgi-bin/cmd>

Table 2. Derived fundamental parameters of the studied star clusters.

Star Cluster	$(m - M)_0$ (mag)	d (kpc)	[Fe/H] (dex)	Log(age /yr)	SMC region ^a
B88	18.94 ± 0.17	61.38 ± 4.74	-0.25 ± 0.16	8.12 ± 0.16	Counter Bridge
B99	17.90 ± 0.08	38.02 ± 1.38	-0.86 ± 0.04	8.6 ± 0.12	Main Body
B139	18.83 ± 0.26	58.34 ± 6.89	-0.27 ± 0.21	8.10 ± 0.35	Northern Bridge
B168	18.80 ± 0.11	57.54 ± 2.64	-1.04 ± 0.07	9.82 ± 0.06	Northern Bridge
BS116	18.73 ± 0.14	55.72 ± 3.54	-0.68 ± 0.12	9.26 ± 0.05	Main Body
BS121	19.38 ± 0.01	75.16 ± 0.34	-0.78 ± 0.01	9.42 ± 0.01	Main Body
BS188	18.51 ± 0.31	50.35 ± 7.09	-0.90 ± 0.10	9.15 ± 0.10	Northern Bridge
H8697	17.83 ± 0.20	36.81 ± 3.35	-0.73 ± 0.02	8.27 ± 0.12	Main Body
HW31	18.70 ± 0.10	54.95 ± 2.50	-0.90 ± 0.05	9.66 ± 0.06	Southern Bridge
HW41	18.60 ± 0.05	52.48 ± 1.19	-0.75 ± 0.01	9.61 ± 0.02	Main Body
HW47	18.70 ± 0.06	54.95 ± 1.50	-0.90 ± 0.02	9.40 ± 0.02	Southern Bridge
HW56	18.80 ± 0.13	57.54 ± 3.40	-0.73 ± 0.09	9.46 ± 0.05	Northern Bridge
HW64	19.25 ± 0.22	70.79 ± 7.08	-0.37 ± 0.26	7.49 ± 0.28	Northern Bridge
HW67	18.63 ± 0.05	53.21 ± 1.21	-0.70 ± 0.07	9.28 ± 0.04	Northern Bridge
HW73	18.79 ± 0.19	57.28 ± 4.95	-0.50 ± 0.23	8.16 ± 0.11	Northern Bridge
HW77	18.91 ± 0.05	60.53 ± 1.38	-0.75 ± 0.06	9.05 ± 0.02	Bridge
HW84	18.30 ± 0.08	45.71 ± 1.66	-0.86 ± 0.02	9.32 ± 0.02	Northern Bridge
HW86	18.55 ± 0.04	51.29 ± 0.93	-0.54 ± 0.02	9.15 ± 0.02	Bridge
IC1655	18.76 ± 0.06	56.49 ± 1.54	-0.58 ± 0.05	8.30 ± 0.14	Northern Bridge
L2	18.88 ± 0.06	59.70 ± 1.63	-1.34 ± 0.06	9.67 ± 0.02	West Halo
L3	18.52 ± 0.07	50.58 ± 1.61	-0.93 ± 0.08	9.15 ± 0.03	West Halo
L4	18.76 ± 0.02	56.49 ± 0.51	-1.14 ± 0.08	9.85 ± 0.01	West Halo
L6	18.60 ± 0.10	52.48 ± 2.39	-1.28 ± 0.07	9.67 ± 0.02	West Halo
L7	18.76 ± 0.09	56.49 ± 2.31	-0.88 ± 0.07	9.13 ± 0.09	West Halo
L9	18.75 ± 0.04	56.23 ± 1.02	-0.65 ± 0.03	9.29 ± 0.02	West Halo
L11	18.87 ± 0.07	59.43 ± 1.89	-0.93 ± 0.05	9.44 ± 0.01	West Halo
L13	18.59 ± 0.03	52.24 ± 0.71	-1.18 ± 0.04	8.97 ± 0.01	West Halo
L17	18.60 ± 0.21	52.48 ± 5.01	-0.80 ± 0.07	9.64 ± 0.05	Main Body
L19	18.75 ± 0.08	56.23 ± 2.04	-0.93 ± 0.05	9.48 ± 0.03	Main Body
L27	18.82 ± 0.08	58.07 ± 1.81	-1.10 ± 0.04	9.68 ± 0.05	Main Body
L58	18.64 ± 0.04	53.46 ± 0.97	-0.80 ± 0.01	9.25 ± 0.02	Southern Bridge
L73	18.89 ± 0.22	59.98 ± 6.01	-0.63 ± 0.16	9.27 ± 0.03	Counter Bridge
L95	19.08 ± 0.07	65.46 ± 2.08	-0.34 ± 0.04	7.96 ± 0.15	Northern Bridge
L100	18.73 ± 0.03	55.72 ± 0.76	-0.65 ± 0.05	9.52 ± 0.01	Northern Bridge
L108	18.67 ± 0.11	54.20 ± 2.71	-0.82 ± 0.11	9.30 ± 0.10	Northern Bridge
L110	18.70 ± 0.06	54.95 ± 1.50	-0.98 ± 0.03	9.78 ± 0.01	Bridge
L116	18.13 ± 0.17	42.27 ± 3.27	-1.14 ± 0.08	9.39 ± 0.05	Southern Bridge
NGC416	18.92 ± 0.02	60.81 ± 0.46	-1.22 ± 0.02	9.81 ± 0.06	Main Body
NGC458	18.67 ± 0.09	54.20 ± 2.22	-0.59 ± 0.07	8.12 ± 0.027	Northern Bridge
OGLE-CL SMC 133	18.54 ± 0.04	51.05 ± 0.93	-0.88 ± 0.04	9.33 ± 0.03	Main Body

^a From Dias et al. (2014) and Dias et al. (2016).

more weight. For completeness purposes, we also included fundamental parameters values found in the literature that we consider not as accurate as our present ones (B139, HW73). Table 1 lists the adopted average values. We here estimated accurate heliocentric distances, for the first time, for nearly 40 per cent of

the studied clusters. This outcome points to the need of an observational campaign to perform a deep imaging survey to definitively tackle the 3D spatial distribution of the SMC cluster population from accurate heliocentric distance for a statistical significant SMC cluster sample. At present less than 5 per cent of the

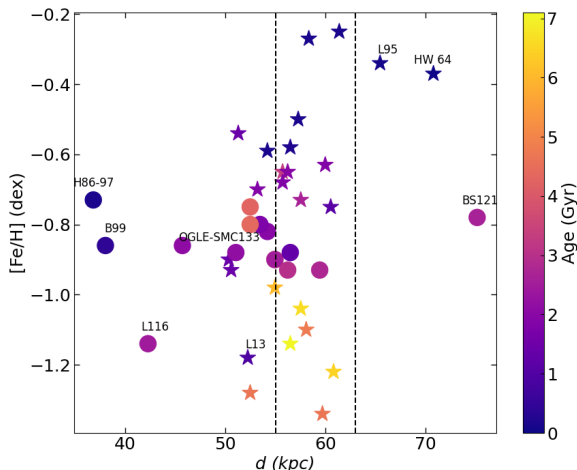


Fig. 6. Relationship between the derived metallicities and heliocentric distances of the studied star clusters, colored according to their derived ages. Filled stars and circles represent star clusters with or without previous estimates of their heliocentric distances, respectively. The vertical dashed lines delimit the extension of the SMC Main Body (Piatti 2023).

cataloged SMC star cluster population has some individual heliocentric distance estimate (Piatti 2023). As mentioned above, until recently, photometric studies of SMC clusters assumed the SMC mean distance modulus. Such an assumption was valid in the context of a poorer photometric data, which did not distinguish distance variation of ~ 4.7 kpc ($\Delta(\text{distance modulus}) \sim 0.16$ mag); the FWHM of the SMC Main Body (Graczyk et al. 2020).

Figures 3 to 5 show a comparison between our resulting true distance moduli, ages and metallicities with those found in the literature, respectively. We did not include in Figure 3 B139 and HW 73 because the available distance moduli are not as accurate as our present estimates (this can be checked by visually comparing Figure 2 of Piatti (2022) with the corresponding ones in the Appendix. As can be seen, all three parameters show a very good agreement, the difference being $\Delta(\log(\text{age}/\text{yr})_{\text{our}} - \log(\text{age}/\text{yr})_{\text{lit.}}) = 0.09 \pm 0.07$, $\Delta([\text{Fe}/\text{H}]_{\text{our}} - [\text{Fe}/\text{H}]_{\text{lit.}}) = 0.073 \pm 0.051$ dex, and $\Delta((m-M)_{\text{our}} - (m-M)_{\text{lit.}}) = 0.14 \pm 0.06$ mag, respectively.

3.1. Some selected star clusters

In this section we focus on the most prominent star clusters included in our sample without prior estimates of their heliocentric distance, with the aim of describing our resulting parameters in some detail.

For B99 we derive a mean true distance modulus of 17.9 mag, which in turn implies a mean heliocentric distance $d = 38.02$ kpc; mean cluster age and metallicity resulted to be 0.39 Gyr and $[\text{Fe}/\text{H}] = -0.86$, respectively. Our derived age is slightly larger than that obtained by Maia et al. (2014) (0.12 Gyr), while we found an excellent agreement with the spectroscopic metallicity value derived by Parisi et al. (2015) ($[\text{Fe}/\text{H}] = -0.84$ dex).

The best-fitted theoretical isochrone for BS121 corresponds to an age of 2.63 Gyr and an overall metal content $[\text{Fe}/\text{H}] = -0.78$ dex, for a true distance modulus of 19.38 mag ($d = 75.16$ kpc). Both estimated cluster age and metallicity are in very good agreement with the values obtained by Parisi et al. (2009) and Parisi et al. (2015).

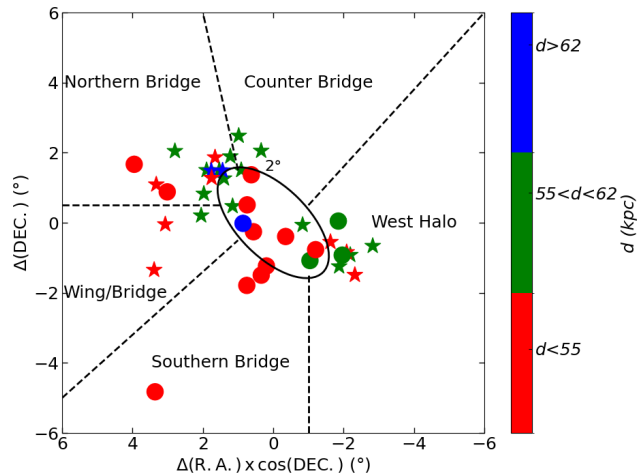


Fig. 7. Distribution in the sky of the studied SMC star clusters. Colored symbols are according to the star cluster heliocentric distances. Dashed lines delimit the different outermost SMC regions (see text for details). Filled stars and circles represent star clusters with or without previous estimates of their heliocentric distances, respectively.

The CMD of H86-97 was satisfactorily reproduced by an isochrones of age = 0.19 Gyr and $[\text{Fe}/\text{H}] = -0.73$ dex, for a mean true distance modulus of 17.83 mag ($d = 36.81$ kpc). Our estimated age resulted to be slightly younger than the age derived by Chiosi et al. (2006) (0.32 Gyr), while the present cluster metal content agrees well with the Ca II triplet metallicity obtained by Parisi et al. (2015).

The isochrone which best reproduces the CMD of OGLE-SMC 133 is that of an age of 2.14 Gyr, $[\text{Fe}/\text{H}] = -0.88$ dex and true distance modulus of 18.54 mag (51.05 kpc). Although the resulting metallicity is in agreement with that of Parisi et al. (2015) ($[\text{Fe}/\text{H}] = -0.80$ dex), our cluster age resulted slightly younger than the value obtained by Glatt et al. (2010) (6.29 Gyr).

The ages and metallicities of L7, L19, L58 and L116 are in very good agreement with the values retrieved from the literature (see Tables 1 and 2), while the derived mean true distance moduli are 18.76 mag ($d = 56.49$ kpc), 18.75 mag ($d = 56.23$ kpc), 18.64 mag ($d = 53.46$ kpc), and 18.13 mag ($d = 42.27$ kpc), respectively.

4. Analysis and discussion

In the subsequent analysis we discuss the relationship between the clusters' ages and metallicities with their positions in the SMC, in the context of the galaxy formation, and its chemical and dynamical evolution. Our goal is to investigate whether star clusters projected toward tidally perturbed/induced SMC regions already formed therein, and from the confirmed ones to assess whether these regions are detachments of the old outer SMC disk or have been formed recently.

Figure 6 shows the variation of the derived metallicities with the cluster heliocentric distances. For the sake of the reader, we represented the SMC Main Body boundaries with two vertical dashed lines. They come from the best-fitted rotation disk of SMC star clusters obtained by Piatti (2021). As can be seen, there is a remarkable percentage of the studied star cluster sample that is located beyond those limits, preferentially toward closer distances. The derived distances uncover a spatial distri-

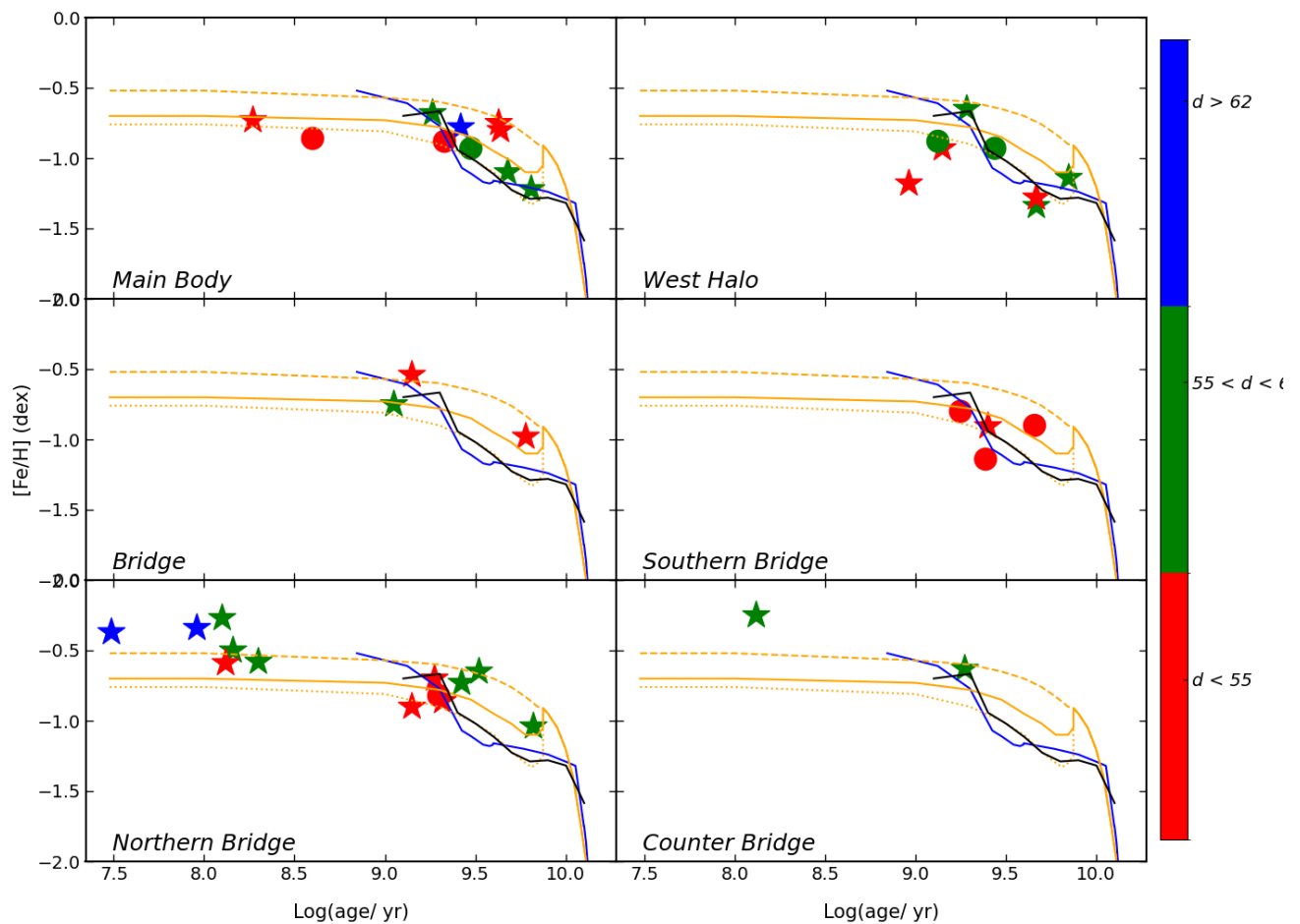


Fig. 8. Age-metallicity relationship for different SMC regions. Symbols are as in Figure 7. The observed age-metallicity relationship of Piatti & Geisler (2013), and the theoretical ones computed by Pagel & Tautvaisiene (1998) and Tsujimoto & Bekki (2009) are superimposed with black, blue, and orange lines, respectively. The dashed and solid orange lines correspond to cases without merger and with a merger of two similar mass galaxies, respectively.

bution of SMC star clusters, in agreement with other independent studies that support the stripping scenario, originated by the tidal interaction with the Large Magellanic Cloud (LMC) (Subramanian et al. 2017; Cullinane et al. 2023; Nidever 2024). SMC outer disk star clusters have long been commonly thought to be old and hence, to be key to reconstructing the early galaxy formation and chemical enrichment history, while young star clusters are expected to be found in the inner galaxy region, where still remain gas and dust. From these points of view, the older and more metal-poor star clusters located in the outer SMC disk, as well as those younger and more metal-rich placed in the inner galaxy, should not call our attention. However, the two closest star clusters to the Sun (H86-97 and B99) and two other clusters located behind the SMC Main Body (L95 and HW64) are young star clusters, which strikes our understanding about their roles in the galaxy formation and evolution processes. Notably, both young star clusters located behind the SMC formed from a more chemically enriched material than their counterparts closer to the Sun. Nevertheless, for the bulk of the studied star clusters, the younger a star cluster the more metal-rich, in agreement

with the observed SMC cluster age-metallicity relationship (Piatti 2011).

Carpintero et al. (2013) modeled the dynamical interaction between the SMC and the LMC and their corresponding stellar cluster populations. Their simulations probing a wide range of parameters for the orbits of both galaxies showed that approximately 15 per cent of the SMC clusters are captured by the LMC. In addition, another 20-50 per cent of its clusters are ejected into the intergalactic medium. These results pave our understanding of the observed spatial distribution of the studied star clusters as objects that could have been reached by the tidal interactions between both Magellanic Clouds. Indeed, The LMC is located closer to the Sun than the SMC, so that some SMC star clusters with heliocentric distances smaller than the mean SMC distance could have experienced stripped from the LMC. Accompanying evidence of such an effect was found by Piatti & Lucchini (2022), who analyzed SMASH (Nidever et al. 2021) and *Gaia* EDR3 (Gaia Collaboration et al. 2016, 2020) data of the recently discovered star cluster YMCA-1, to conclude that it formed in the SMC and then stripped by the LMC. YMCA-1 is a 9.6 Gyr

old and moderately metal-poor ($[\text{Fe}/\text{H}] = -1.16$ dex) star cluster located at 60.9 kpc from the Sun, and at ~ 17.1 kpc to the East from the LMC center.

Dias et al. (2014) and Dias et al. (2016) defined different zones throughout the outermost SMC regions, called: Northern Bridge, Counter Bridge, West Halo, Southern Bridge and Wing/Bridge, respectively (see Figure 1 in Dias et al. 2022). For comparison purposes, we have superimposed them in Figure 7. As can be seen, all of them are populated by star clusters analyzed in this work. In the Figure we have distinguished star clusters with or without previous heliocentric distance estimates using filled stars and circles, respectively. We employed the heliocentric distances of the star clusters as indicators of the tidally perturbed/induced origin of the outermost SMC regions where they appear, and considered for our analysis three different distance cuts, namely, star clusters located closer than 55 kpc, between 55 kpc and 62 kpc, and beyond 62 kpc, according to Piatti (2021) (see also Figure 6).

The Northern and Southern Bridges and the Wing/Bridge regions contain studied star clusters located in front of the SMC Main Body, which support their tidal origin. These regions are facing the LMC, which is at ~ 50 kpc from the Sun (de Grijs et al. 2014), so that it would seem that exists a vast region between both galaxies connecting them. This outcome is in very good agreement with the results obtained by Wagner-Kaiser & Sarajedini (2017), who derived metallicity and distance distributions of RR Lyrae variables stars to probe the structure of the Magellanic system as a whole, revealing a smooth transition that connects the galaxies. Star clusters closer than 55 kpc from the Sun are also seen toward the SMC Main Body, inside an ellipse of 2° . These star clusters confirm the larger extension of the galaxy along the line-of-sight, with a 1:2:4 3D shape, being the declination, right ascension and line-of-sight the three axes, respectively (Ripepi et al. 2017; Muraveva et al. 2018). Likewise, star clusters farther than 62 kpc from the Sun are observed in the Northern Bridge and projected toward the SMC Main Body.

Besides the cluster heliocentric distances, the cluster ages and metallicities also play a role that sheds light on to the origin of the SMC stellar structures where the clusters belong to. In this sense, comparing the SMC age-metallicity relationship (AMR) with those of the aforementioned outermost regions contribute to understand at what extend these regions have chemically evolved differently from the SMC. For comparison purposes, we used the AMR derived by Piatti & Geisler (2013) from Washington photometry of field stars distributed throughout the whole galaxy, and the theoretical ones computed by Pagel & Tautvaisiene (1998) and Tsujimoto & Bekki (2009), respectively. Pagel & Tautvaisiene (1998) predicted an intensive star formation and chemical enrichment during the SMC formation epoch and a rapid burst of chemical enrichment about 3 Gyr ago. On the other hand, Tsujimoto & Bekki (2009) predicted a major merger at ~ 7.5 Gyr ago between two small galaxies of similar mass. Figure 8 depicts the resulting AMR for different outermost SMC regions with star clusters colored according to their heliocentric distances.

In general, the studied clusters located in different SMC regions follow the overall SMC AMR. The most discordant star cluster would seem to be L13, located in the West Halo ($\log(\text{age}/\text{yr}) = 8.97$, $[\text{Fe}/\text{H}] = -1.18$ dex). Its relatively low metal content could suggest that it formed from not-well mixed gas. Star clusters located at heliocentric distances < 55 kpc do not distinguish chemically from those populating the SMC Main Body. From this outcome we speculate with the possibility that they could have formed in the SMC and then migrated beyond the galaxy

periphery dragged by the tidal effects caused by the LMC/SMC interaction. In addition, relatively young and distant clusters ($55 \text{ kpc} > d > 62 \text{ kpc}$) located in the Northern Bridge tell us that enriched gas has also reached the outermost SMC regions.

5. Conclusions

The SMC is known to have experienced tidal effects from its interaction with the LMC. As expected, its star cluster population has not been indifferent to such an interaction history, which can be deciphered from the relationship between their ages, metallicities and distances. To this respect, we selected 40 SMC star clusters aiming at deriving their astrophysical properties, from which to look for the connection between the star clusters and the tidally perturbed/induced outermost SMC regions where they are located. We used relatively deep cluster CMDs built from SMASH DR2 photometry and, once they were properly cleaned from the field star contamination, we derived their cluster fundamental parameters.

We found that the homogeneously derived clusters' ages, heliocentric distances and metallicities are put on a uniform scale validated by published reliable estimates. We obtained for the first time heliocentric distances for 15 star clusters, which represents an increase of ~ 50 per cent of the number of SMC clusters pertaining to the group of clusters with derived distances (Piatti 2023); the SMC containing more than 650 star clusters (Bica et al. 2020). This small sample of clusters with heliocentric distances are distributed throughout the SMC Main Body, similarly as field stars do. For this reason, finding star clusters beyond the SMC body triggers the speculation that they could have been stripped from the interaction with the LMC.

When dealing with the estimated cluster heliocentric distances, we found that nearly half of the studied star clusters are located beyond the SMC Main Body. Most of them are in front of the SMC, but there are some ones also located behind it. This result is not unexpected, bearing in mind independent observational evidence of the tidal interaction between the LMC and the SMC. Here we confirm the existence of that physical connection between both galaxies, using star clusters as tracers.

From the analysis of the AMRs of star clusters located in different outermost SMC regions, and in the Main Body of the galaxy, we found that intermediate-age and old star clusters follow in general the overall galaxy chemical enrichment history. Since some of them are placed at the present time beyond the SMC Main Body boundaries, we conclude that they could have traveled outward under the effects of the tidal interaction between the Magellanic Clouds. Moreover, not only star clusters formed in the SMC have surpassed its outskirts, but also chemically enriched gas. This is supported by the formation of young metal-rich star clusters in the Northern Bridge that also span a wide range of heliocentric distances. Therefore, the SMC has become a dwarf galaxy scarred by LMC tidal effects with distance-perturbed and newly induced (formed) outermost stellar structures. Precisely, not considering such a complex galaxy reality could mislead our understanding of the formation and evolution of the SMC, for example, the present spatial distribution of the star cluster metal content.

Acknowledgements. We thank the referee for the thorough reading of the manuscript and timely suggestions to improve it. This research uses services or data provided by the Astro Data Lab at NSF's National Optical-Infrared Astronomy Research Laboratory. NSF's OIR Lab is operated by the Association of Universities for Research in Astronomy (AURA), Inc. under a cooperative agreement with the National Science Foundation. Data for reproducing the figures and analysis in this work will be available upon request to the first author.

References

- Alcaino, G., Alvarado, F., Borissova, J., & Kurtev, R. 2003, *Astronomy & Astrophysics*, 400, 917
- Almeida, A., Majewski, S. R., Nidever, D. L., et al. 2024, *Monthly Notices of the Royal Astronomical Society*, 529, 3858
- Bica, E., Westera, P., Kerber, L. d. O., et al. 2020, *AJ*, 159, 82
- Bica, E., Westera, P., Kerber, L. d. O., et al. 2020, *VizieR Online Data Catalog*, J Bressan, A., Marigo, P., Girardi, L., et al. 2012, *Monthly Notices of the Royal Astronomical Society*, 427, 127
- Carpintero, D. D., Gomez, F. A., & Piatti, A. E. 2013, *MNRAS*, 435, L63
- Chiosi, E., Vallenari, A., Held, E., Rizzi, L., & Moretti, A. 2006, *Astronomy & Astrophysics*, 452, 179
- Cullinane, L., Mackey, A., Da Costa, G., Koposov, S. E., & Erkal, D. 2023, *Monthly Notices of the Royal Astronomical Society: Letters*, 518, L25
- De Bortoli, B. J., Parisi, M. C., Bassino, L. P., et al. 2022, *Astronomy & Astrophysics*, 664, A168
- De Grijs, R., & Bono, G. 2015, *The Astronomical Journal*, 149, 179
- de Grijs, R., Wicker, J. E., & Bono, G. 2014, *AJ*, 147, 122
- De Leo, M., Carrera, R., Noël, N. E., et al. 2020, *Monthly Notices of the Royal Astronomical Society*, 495, 98
- Di Teodoro, E. M., McClure-Griffiths, N., Jameson, K., et al. 2019, *Monthly Notices of the Royal Astronomical Society*, 483, 392
- Dias, B., Angelo, M. S., Oliveira, R. A. P. d., et al. 2021, *Astronomy & Astrophysics*, 647, L9
- Dias, B., Kerber, L., Barbuy, B., Bica, E., & Ortolani, S. 2016, *Astronomy & Astrophysics*, 591, A11
- Dias, B., Kerber, L. d. O., Barbuy, B., et al. 2014, *Astronomy & Astrophysics*, 561, A106
- Dias, B., Parisi, M. C., Angelo, M., et al. 2022, *Monthly Notices of the Royal Astronomical Society*, 512, 4334
- Efron, B. 1982, *The Jackknife, the bootstrap and other resampling plans* (SIAM)
- Gaia Collaboration, Luri, X., Chemin, L., et al. 2020, *arXiv e-prints*, arXiv:2012.01771
- Gaia Collaboration, Prusti, T., de Bruijne, J. H. J., et al. 2016, *A&A*, 595, A1
- Gatto, M., Ripepi, V., Bellazzini, M., et al. 2021, *Monthly Notices of the Royal Astronomical Society*, 507, 3312
- Glatt, K., Grebel, E. K., & Koch, A. 2010, *Astronomy & Astrophysics*, 517, A50
- Glatt, K., Grebel, E. K., Sabbi, E., et al. 2008, *The Astronomical Journal*, 136, 1703
- Graczyk, D., Pietrzyński, G., Thompson, I. B., et al. 2020, *The Astrophysical Journal*, 904, 13
- Kallivayalil, N., Van der Marel, R. P., Besla, G., Anderson, J., & Alcock, C. 2013, *The Astrophysical Journal*, 764, 161
- Kroupa, P. 2002, *Science*, 295, 82
- Livanou, E., Dapergolas, A., Kontizas, M., et al. 2013, *Astronomy & Astrophysics*, 554, A16
- Maia, F., Piatti, A. E., & Santos Jr, J. F. 2014, *Monthly Notices of the Royal Astronomical Society*, 437, 2005
- Maia, F. F., Dias, B., Santos Jr, J. F., et al. 2019, *Monthly Notices of the Royal Astronomical Society*, 484, 5702
- Milone, A. P., Cordoni, G., Marino, A., et al. 2023, *Astronomy & Astrophysics*, 672, A161
- Muraveva, T., Subramanian, S., Clementini, G., et al. 2018, *MNRAS*, 473, 3131
- Narloch, W., Pietrzyński, G., Gieren, W., et al. 2021, *Astronomy & Astrophysics*, 647, A135
- Nayak, P., Subramanian, A., Choudhury, S., & Sagar, R. 2018, *Astronomy & Astrophysics*, 616, A187
- Nidever, D. L. 2024, *MNRAS*, 533, 3238
- Nidever, D. L., Olsen, K., Choi, Y., et al. 2021, *AJ*, 161, 74
- Niederhofer, F., Cioni, M.-R., Rubele, S., et al. 2018, *Astronomy & Astrophysics*, 613, L8
- Niederhofer, F., Cioni, M.-R. L., Rubele, S., et al. 2021, *Monthly Notices of the Royal Astronomical Society*, 502, 2859
- Oliveira, R., Maia, F., Barbuy, B., et al. 2023, *Monthly Notices of the Royal Astronomical Society*, 524, 2244
- Pagel, B. E. J. & Tautvaisiene, G. 1998, *MNRAS*, 299, 535
- Parisi, M., Grocholski, A., Geisler, D., Sarajedini, A., & Clariá, J. 2009, *The Astronomical Journal*, 138, 517
- Parisi, M. C., Geisler, D., Carraro, G., et al. 2014, *The Astronomical Journal*, 147, 71
- Parisi, M. C., Geisler, D., Clariá, J. J., et al. 2015, *The Astronomical Journal*, 149, 154
- Parisi, M. C., Gramajo, L. V., Geisler, D., et al. 2022, *Astronomy & Astrophysics*, 662, A75
- Perren, G. I., Vazquez, R. A., & Piatti, A. E. 2015, *Astronomy & Astrophysics*, 576, A6
- Piatti, A. E. 2011, *MNRAS*, 418, L69
- Piatti, A. E. 2021, *Astronomy & Astrophysics*, 650, A52
- Piatti, A. E. 2022, *Monthly Notices of the Royal Astronomical Society*, 509, 3462
- Piatti, A. E. 2023, *Monthly Notices of the Royal Astronomical Society*, 526, 391
- Piatti, A. E. & Bica, E. 2012, *Monthly Notices of the Royal Astronomical Society*, 425, 3085
- Piatti, A. E., Clariá, J. J., Bica, E., et al. 2011, *Monthly Notices of the Royal Astronomical Society*, 417, 1559
- Piatti, A. E. & Geisler, D. 2013, *AJ*, 145, 17
- Piatti, A. E. & Lucchini, S. 2022, *MNRAS*, 515, 4005
- Piatti, A. E., Santos Jr, J. F., Clariá, J. J., et al. 2001, *Monthly Notices of the Royal Astronomical Society*, 325, 792
- Piatti, A. E., Sarajedini, A., Geisler, D., Gallart, C., & Wischnjewsky, M. 2007, *Monthly Notices of the Royal Astronomical Society*, 382, 1203
- Piatti, A. E., Sarajedini, A., Geisler, D., Seguel, J., & Clark, D. 2005, *Monthly Notices of the Royal Astronomical Society*, 358, 1215
- Ripepi, V., Cioni, M.-R. L., Moretti, M. I., et al. 2017, *Monthly Notices of the Royal Astronomical Society*, 472, 808
- Saroon, S., Dias, B., Tsujimoto, T., et al. 2023, *Astronomy & Astrophysics*, 677, A35
- Subramanian, S., Rubele, S., Sun, N.-C., et al. 2017, *MNRAS*, 467, 2980
- Tsujimoto, T. & Bekki, K. 2009, *ApJ*, 700, L69
- Wagner-Kaiser, R. & Sarajedini, A. 2017, *Monthly Notices of the Royal Astronomical Society*, 466, 4138
- Zivick, P., Kallivayalil, N., & van der Marel, R. P. 2021, *The Astrophysical Journal*, 910, 36
- Zivick, P., Kallivayalil, N., van der Marel, R. P., et al. 2018, *The Astrophysical Journal*, 864, 55

Appendix A: Cleaned CMDs with the corresponding theoretical isochrones

